J Appl Electrochem (2008) 38:297–308
DOI 10.1007/s10800-007-9438-6

ORIGINAL PAPER

Hydrogen filter press electrolyser modelled by coupling Fluent® and Flux Expert® codes

F. Jomard · J. P. Feraud · J. Morandini · Y. Du Terrail Couvat · J. P. Caire

Received: 2 March 2007 / Revised: 4 October 2007 / Accepted: 22 October 2007 / Published online: 17 November 2007

Abstract Mass production of hydrogen is a major issue for the coming decades particularly to decrease greenhouse gas production. The development of fourth-generation high-temperature nuclear reactors has led to renewed interest for hydrogen production. In France, the CEA is investigating new processes using nuclear reactors, such as the Westinghouse hybrid cycle. A recent study was devoted to electrical modeling of the hydrogen electrolyzer, which is the key unit of this process. In this electrochemical reactor, hydrogen is reduced at the cathode and SO_2 is oxidized at the anode with the advantage of a very low voltage cell. This paper describes an improved model coupling the electrical and thermal phenomena with hydrodynamics in the electrolyzer, designed for a priori computational optimization of our future pilot cell. The hydrogen electrolyzer chosen here is a filter press design comprising a stack of identical cathode and anode compartments separated by a membrane. In a complex reactor of this type the main coupled physical phenomena involved are forced convection of the electrolyte flows, the plume of evolving hydrogen bubbles that modifies the local electrolyte conductivity, and all the irreversible processes that contribute to local overheating (Joule effect, overpotentials, etc.). The secondary current distribution was modeled with a commercial FEM code, Flux Expert®, which was customized with specific finite interfacial elements capable of describing the potential discontinuity associated with the electrochemical overpotential. Since the finite element method is not capable of properly describing the complex two-phase flows in the cathode compartment, the Fluent® CFD code was used for thermohydraulic computations. In this way each physical phenomenon was modeled using the best numerical method. The coupling implements an iterative process in which each code computes the physical data it has to transmit to the other one: the two-phase thermohydraulic problem is solved by Fluent® using the Flux-Expert® current density and heat sources; the secondary distribution and heat losses are solved by Flux-Expert® using the Fluent® temperature field and flow velocities. A set of dedicated library routines was developed for process initiation, message passing, and synchronization of the two codes. The first results obtained with the two coupled commercial codes give realistic distributions for the electrical current density, gas fraction, and velocity in the electrolyzer. This approach allows us to optimize the design of a future experimental device.

Keywords Numerical model · Westinghouse cycle · Coupling · Hydrogen electrolyzer · Fluent · Flux Expert

F. Jomard · J. P. Feraud
CEA Valrhô, DTEC/SGCS/LGCI, BP 17171, 30207 Bagnols sur Cèze, France

J. Morandini
Astek Rhone-Alpes, 1 place du Verseau, 38130 Echirolles, France

Y. Du Terrail Couvat
Laboratoire Simap, Enseeg, BP 75, 38402 St Martin d'Hères cedex, France

J. P. Caire (✉)
LEPMI, ENSEEG, 1130 Rue de la Piscine, 38402 Saint Martin d'Hères, France
e-mail: jean-pierre.caire@lepmi.inpg.fr

Notation

Cp	Heat capacity (J kg^{-1} K^{-1})
$\vec{g}$	Gravitational acceleration (m s^{-2})
$\vec{J}$	Current density (A m^{-2})

j_n	Current density normal to the interface (A m^{-2})
k	Thermal conductivity (W m^{-1} K^{-1})
$\vec{n}$	Normal vector
NBN	Number of integration points
Q_S	Surface heat sources (W m^{-2})
Q_V	Volume heat sources (W m^{-3})
T	Temperature (K)
t	Time (s)
$\vec{u}$	Velocity vector (m s^{-1})
u, v	Relative coordinates
V	Electrical scalar potential (V)
$\alpha(u, v)$, γ, β	Lagrange polynomials
δ	Nanometric discontinuity thickness of potential (m)
δ_S	Dirac surface distribution
ε_g	Gas fraction
ρ	Density (kg m^{-3})
η	Overpotential (V)
$\overline{\overline{\sigma}}$	Viscous stress tensor (Pa)
σ	Electrical conductivity (Ω^{-1} m^{-1})
$\vec{\nabla}$	Nabla vector differential operator ($\partial_x\bullet, \partial_y\bullet, \partial_z\bullet$)

1 Introduction

Mass production of hydrogen is a major issue for the coming decades as part of a policy of progress and sustainability, particularly to decrease greenhouse gas production. The key advantage of hydrogen is that no carbon dioxide (CO_2) is produced at the tailpipe when hydrogen is burned. Unlike nuclear and solar power, hydrogen can be used directly as fuel. Hydrogen fuel cell cars could represent a breakthrough in the next decade requiring a large and low cost industrial production of hydrogen.

Within the framework of the Generation IV International Forum the *Commissariat à l'Énergie Atomique* (CEA) is investigating the possibility of producing hydrogen in industrial quantities. One of the main objectives is to take advantage of the very high-temperature heat source of 1100 K obtained at a reasonable cost by future nuclear reactors such as the Very High Temperature Reactor [1, 2]. Large-scale hydrogen production is also being considered using hybrid cycles such as the Westinghouse Sulphur Cycle, which is based on sulphur dioxide oxidation and an electrochemical reduction of protons to form hydrogen [3, 4]. Agranat et al. [5] recently highlighted the interest of coupling gas/liquid CFD and experimental investigation as a cost-effective and reliable design tool for high-pressure electrolyzer hydrogen production. Computational modeling is also particularly attractive for enhancing the electrolyser competitiveness, in terms of design and energy consumption, to provide a large-scale and low-cost hydrogen production.

This paper describes the work carried out to model and optimize a filter press electrolyser [6] for producing hydrogen via the Westinghouse hybrid cycle [7]. Considering the cost and complexity of fabricating a filter press electrolyser, numerical modelling proved to be a valuable tool for the preliminary design of a prototype unit. This modelling approach consists in developing a predictive tool for understanding the electrochemical behaviour of the electrolyser when hydrogen bubbles are generated. In view of the complexity of the strongly coupled phenomena that occur in this type of device, no numerical method is currently capable of satisfactorily describing both the thermo hydraulic and electrochemical aspects of the electrolyser. The original idea behind this work was to account for the coupled physical phenomena by coupling two software packages that together are perfectly suitable for describing the physical problems encountered.

The Flux Expert® finite element code and the Fluent® volume element code were coupled to solve a highly nonlinear steady-state problem involving the coupling of electro kinetics, fluid mechanics, and thermal equations. The following algorithm was adopted for this purpose: (i) Solve the electro kinetic equation using the Flux Expert® code; one feature of this model is the use of specific "interfacial finite elements" developed to handle the over potential at the electrode/electrolyte interfaces [8]. (ii) Simultaneously solve the momentum and energy equations of two-phase turbulent in the electrolyte where gas bubbles are generated by electrolysis; this step was performed using one of the recent effective models for compressible and incompressible two-phase fluid flows developed by Fluent®.

The code coupling is handled by a dedicated library developed in C and each calculation is initiated through the following steps: (i) create the models, (ii) load the models in their respective codes, (iii) start the coupled simulation by iterating the computations of Fluent® and Flux Expert®.

2 Westinghouse filter press electrolyser operating principle

The electrolyser is the heart of the process generating hydrogen gas by sulphuric acid electro-reduction. The electrochemical charge balance is obtained by anodic oxidation of sulphur dioxide. The two half-cell reactions at cathode and anode are:

$$2H^+ + 2e^- \rightarrow H_2 \quad (1)$$

$$SO_2 + 2H_2O \rightarrow 2H^+ + H_2SO_4 + 2e^- \quad (2)$$

The overall cell reaction is:

$$SO_2 + 2H_2O \rightarrow H_2 + H_2SO_4 \quad (3)$$

The actual dioxide sulphur oxidation mechanism has not been clearly established, but is discussed by Struk et al. [9]. As the anodic half-cell reaction is characterized by a thermodynamic potential of 0.17 V (Standard Hydrogen Electrode) the Westinghouse sulphur cell voltage is much lower than the 1.23 V_{SHE} of direct water oxidation (H_2O/O_2 couple).

The operating principle of the electrolyser in which reactions 1 and 2 take place is shown in Fig. 1.

In this case, the anodic cell reaction is very interesting because the standard electrical potential of the H_2SO_3/H_2SO_4 couple is only 0.17 V_{SHE}. For a fixed current density, the electric power required for hydrogen generation is therefore much lower when using the sulphur dioxide oxidation reaction. Indeed, this process makes it theoretically possible to save more than 1 V per element (cell) compared to direct water electrolysis, which is considerable from an industrial perspective. In contrast to the power gain, the overall sulphur process design is more complex than for common water electrolysis. For example, electrode corrosion must be prevented by using a noble metal such as platinum.

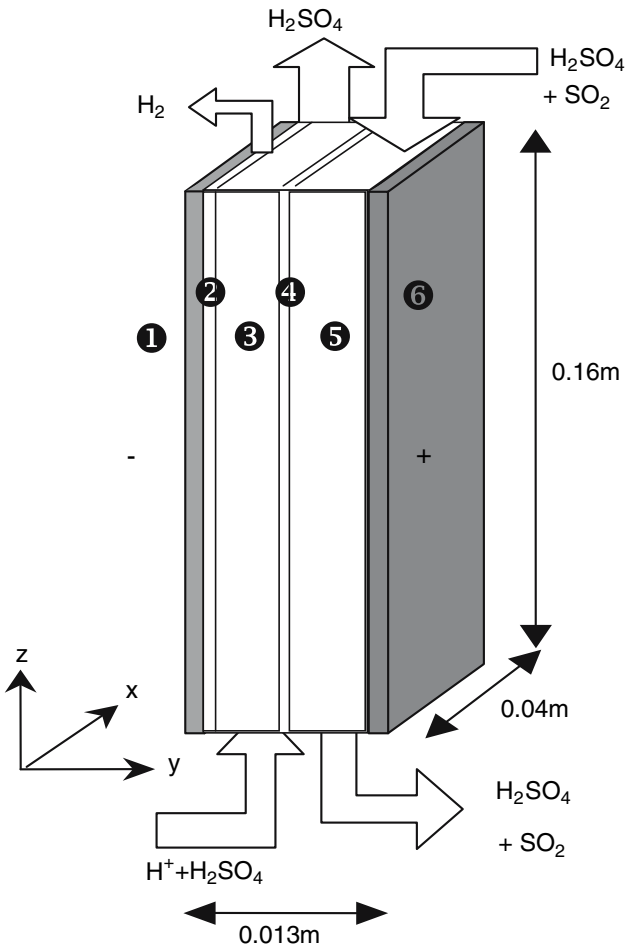

Fig. 1 Electrolyser operating principle (❶ cathode; ❷ hydrogen release zone; ❸ catholyte; ❹ membrane; ❺ anolyte; ❻ anode)

The main difficulties encountered in modelling the electrolyser are due to the various coupling phenomena involved. Our work consists in developing a modelling tool that takes into account all the coupled phenomena to simplify the design of the pre-industrial pilot before construction.

3 Coupling phenomena and electrolyser modelling

The physics of the electrolyser can be described as a two-phase flow thermo hydraulic problem coupled with a secondary current distribution. In the past, each individual physical aspect has been solved by a modelling approach [8, 24, 25]. These physical phenomena are schematically described in the following paragraphs.

3.1 Coupling of physical phenomena

The thermo hydraulic phenomena are described by the Navier–Stokes continuity and heat transfer Eqs. 4–6:

$$\rho\frac{\partial\vec{u}}{\partial t} + \rho(\vec{u}\bullet\vec{\nabla})\vec{u} = \vec{\nabla}\bullet\bar{\bar{\sigma}} + \rho\vec{g} \quad (4)$$

$$\frac{\partial\rho}{\partial t} + \vec{\nabla}\bullet(\rho\vec{u}) = 0 \quad (5)$$

$$\rho c_p\left(\frac{\partial T}{\partial t} + \vec{u}\bullet\vec{\nabla}T\right) + \vec{\nabla}\bullet(-k\vec{\nabla}T) = Q_V + Q_S\delta_S \quad (6)$$

The hydraulic aspect consists of a two-phase problem involving a continuous liquid phase, sulphuric acid, and a dispersed gas phase formed by bubbles generated at the cathode/catholyte interface. The kinetic phenomena taking into account the activation over potentials [11, 12] are described by the charge balance equation and by over potential laws at the electrode/bath interfaces (7):

$$\vec{\nabla}\bullet(-\sigma\vec{\nabla}V) = 0 \quad (7)$$

$$\Delta V = f(\vec{J}\bullet\vec{n}) \quad (8)$$

In Eq. 8 ΔV represents the "over potential" [8–12], i.e. an electrical discontinuity of potential V at the electrode/electrolyte interface. This discontinuity is a true numerical issue for a finite element method that requires the

continuity of V. This problem was overcome previously by the introduction of special interfacial elements in the FEM code Flux Expert® [8]. Equations 4–6 constitute a system of nonlinear partial differential equations with six unknowns: u_x, u_y, P, ε_g, T, V. The nonlinearities are due to the differential operators (the velocity transport term in Eq. 7 for example) but also to the physical properties (overpotentials in particular are described by the logarithmic Tafel law [8]) and the coupling quantities: velocity, local current density at the electrode, temperature, and hydrogen gas volume fraction.

Gas production at the electrode interfaces increases the volume of two-phase fluid flowing in the compartment and thus accelerates the electrolyte velocity. The gas production at level h is proportional to the integral along the electrode of the local current density given by Faraday's law:

$$Q_g(h) = \frac{SM1000\ 3600e}{nFm_V} \int_0^h j(x)dx \tag{9}$$

The evolution of very fine hydrogen bubbles constitutes a plume that modifies the local electrical conductivity of the electrolyte. The electrical conductivity of the two-phase flow is usually described by the Bruggeman formula [14–15]:

$$\sigma(h) = \sigma_0(1 - \varepsilon_g(h))^{3/2} \tag{10}$$

where the gas fraction is:

$$\varepsilon_g(h) = \frac{Q_g(h)}{Q_g(h) + Q_l} \tag{11}$$

Due to the irreversible heat losses (Joule effect and over potentials) all the physical properties depend on the temperature and on the local bubble production. This is particularly well known for the electrical and thermal conductivity of the bath [8]. Solving Eqs. 4–6 thus requires the computation of six variables in two dimensions with strong coupling and constitutes a formidable numerical task.

3.2 Software coupling management

The two types of physical phenomena described above are solved using two codes based on two different numerical methods requiring a priori different qualities and meshes (see Fig. 4). The meshes may be structured or unstructured depending on the calculation domains. Although the hydraulic problem is generally solved under transient conditions and the electro kinetic problem under steady-state conditions, the coupling implemented here must deal with both steady-state and transient problems.

The two-phase flow thermo hydraulic problem is solved using Fluent®, which computes the velocity, pressure, and temperature fields and the gas volume fraction ε_g (bubble concentration) on the finite-volume mesh. Fluent® requires the following inputs (see Table 1)

The following results are provided by Fluent® (see Table 2)

The secondary distribution of current density taking into account the anode and cathode over potentials is solved using Flux Expert®. The code computes the electrical potential and post-processes over the finite element mesh both current density and thermal losses due to Joule effect throughout the cell. Flux Expert® requires the temperature T over the full calculation domain and the gas fraction ε_g in the fluid. The following results are provided by Flux Expert® (see Table 3)

3.3 Data exchange between the two codes

Communication between the two codes is based on the use of a simple and robust message-passing library developed to allow the two calculation codes to communicate without requiring them to be merged into a single executable [13]. The codes can thus be installed on one or even two different UNIX machines. The two programs can share the same physical inputs and results although they use different numerical methods and grids. The message-passing function calls in this library were developed as subroutines in Fluent® and Flux Expert® specially designed for coupling.

Table 1 Inputs required by Fluent

J_n	Current density at the electrode boundary; the current density is used to compute the gas production term at the interface
Q_S	Surface heat sources at the electrode/electrolyte interfaces; this is the source term per unit area in the heat transfer equation corresponding to the heat release related to the overpotential irreversibility
Q_V	The volume heat sources in the electrically conductive zones, i.e. the power density irreversibly generated by Joule effect; this is the volume source term in the heat transfer equation

Table 2 Results provided by Fluent

T	Temperature over the full calculation domain
α_g	Gas concentration in the fluid

Table 3 Results provided by Flux Expert

J, ΔV	Current density and potential at the electrode boundary
Q_S	Surface heat sources in the electrically conductive zones
Q_V	Volume heat sources in the electrically conductive zones

Initially the coordinates of the grid points for which the expected physical quantities will be computed are exchanged by the two programs. Then the coupling data are exchanged throughout the resolution process. Before each iteration, the two codes exchange the values of the physical quantities computed during the preceding step, for those required in the next iteration. The solution strategy data concerns the data that must be exchanged between the programs to reach the same solution: number of iterations, calculated precision, etc., or events such as the end of calculation and the solution output.

The algorithms developed for data sharing are mainly location and interpolation algorithms. Each of the calculation points for the volume and surface heat sources of the Fluent® mesh must be localized on the Flux Expert® mesh. At the beginning of the iterations the heat sources are interpolated over these points and supplied to Fluent®, while the gas volume fraction and temperature must be calculated by Fluent® for the Flux-Expert® mesh points and transmitted to Flux Expert® [13]

The combined operating procedure for the two codes is shown schematically in Fig. 2 where the coupling routines appear in broken line boxes in the flowchart. These routines were developed in C for Flux-Expert and in custom C-like User-Defined Functions (UDF) in Fluent®.

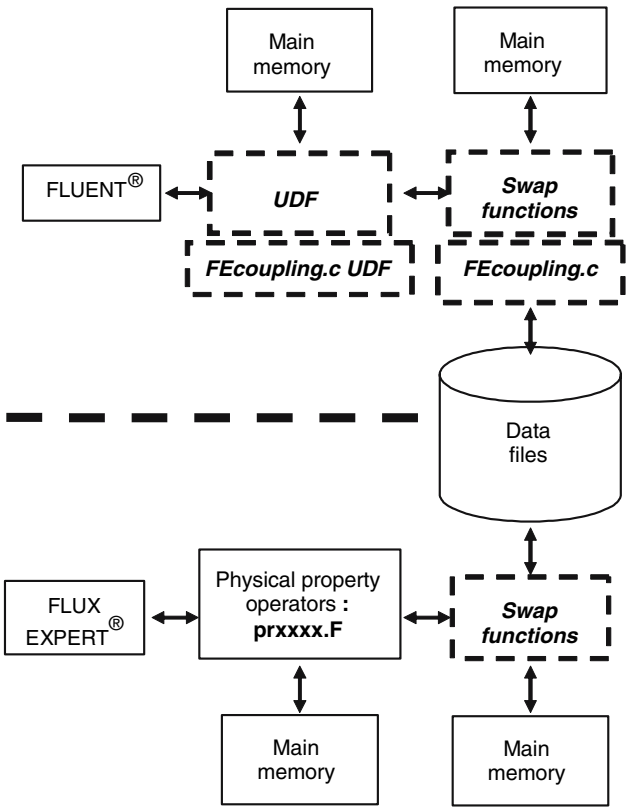

Fig. 2 Fluent®–Flux Expert® coupling flowchart

4 Pilot electrolyser geometry and calculation hypotheses

The filter press electrolyser investigated here (Fig. 1) is a 0.04 × 0.013 × 0.16 m laboratory prototype designed to produce 5 NL h^{-1} of hydrogen. The electrolyser was modelled to partially optimize the design of a small-scale pilot before fabrication. The electrolyser geometric definitions (Fig. 1) for Fluent® and Flux Expert® are practically identical except for the gas release zone at the cathode ❶/catholyte ❸ interface where an additional hydrogen release zone (❷) had to be defined for Fluent® to simulate hydrogen release at the electrode. Within the adjustable thickness of zone ❷ the gas release is calculated according to the local current density. Counter current flow was selected here because it allows greater control over the heat transfer properties of the electrolyser operating as a plate-type filter press heat exchanger.

4.1 Model hypotheses

The future pilot electrolyser was assumed to be a simple rectangular filter press. The study was carried out under steady-state conditions and in three dimensions to properly describe the 3D gas fraction distribution. The physical properties of all the electrolyser components ρ, σ, k, Cp are assumed temperature-dependent since they are partly responsible for the coupling. The anolyte consists only of a single-phase fluid, in this case a sulphuric acid solution. The catholyte consists of a two-phase fluid formed by a sulphuric acid solution with small diameter (about 100 μm) hydrogen bubbles produced by the cathodic electrochemical reaction [9, 10]. The acid concentrations are a priori different in each compartment.

The catholyte conductivity in the presence of evolved bubbles is calculated by the classical Bruggeman equation (10) relating the conductivity to the gas volume fraction ε_g. Furthermore, the gas volume fraction is a function of the hydrogen production (11) related to the height of the electrolyser by Faraday's law (9). The gas generated at level h in the cathode compartment is assumed to be uniformly distributed in the catholyte at this level. Moreover, the gas fraction is assumed sufficiently low throughout the compartment that the current density can be considered constant along the cathode face. This assumption is justified only if the gas volume fraction is everywhere lower than approximately 10% [23, 24].

The outer walls of the electrolyser are thermally insulated. The two fluids with different sulphuric acid concentrations pass through the vertical counter current electrolyser at equivalent rates.

The physical data are representative of the operating conditions frequently described in the literature [7, 10], i.e. a fluid inlet temperature of 323 K at a pressure of 1 bar. The sulphuric acid mass concentrations are 30% in the catholyte and 50% in the anolyte. Most physical data used in this work come from the Westinghouse process experiments reported by Lu et al. [10]. The experimental over potential values at current densities of 2000 A m^{-2} are about 0.6 V at the anode and 0.05 V at the cathode [13]. They are very low compared with other types of electrolysis, resulting in a very low cell voltage in the electrochemical reactor and low energy consumption. This feature is one of the main advantages of the Westinghouse process [8, 9].

4.2 Boundary conditions

The boundary conditions for the two codes are shown in Fig. 3. To simplify the fluid mechanics computations, fluid inlet and outlets placed at right angles in a real filter press were simply assumed axial.

A uniform velocity profile of 0.1 m s^{-1} for electrolyte is therefore applied at the inlets to the cathode and anode compartments. Boundary conditions for evolving bubble velocity are 0.05 and 0.09 m s^{-1} in the Y and Z directions, corresponding to an arbitrary 60° bubbling angle from the cathodic face. The bubble departure angle was previously varied in the range of 30, 45, 60° from the cathodic face; 60° appears to be a suitable value, but this option must still be confirmed experimentally.

4.3 Coupling aspects and meshing bounds

The finite element and finite volume methods require two different meshes since the boundary layers differ for thermo hydraulic and electrochemical phenomena. The quadrangular geometry chosen here allows us to restrict the grid to the use of quadrangles for both methods, even if it is not absolutely indispensable. The 3D electrolyser mesh was prepared in Gambit®. Figure 4 shows the optimum grid used for both thermo hydraulic and electro kinetic modelling.

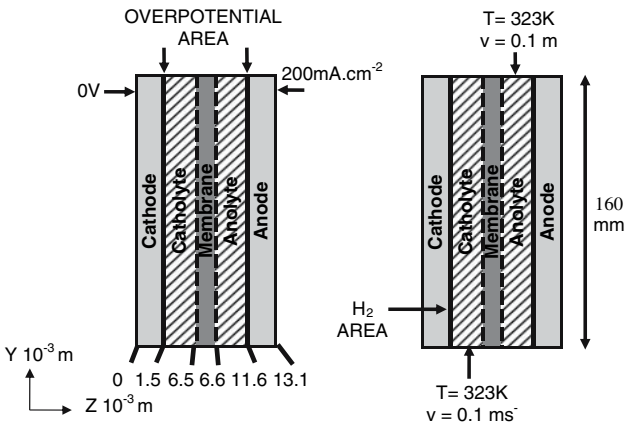

Fig. 3 Boundary conditions Flux-Expert (left) and Fluent (right)

The mesh, comprising 67000 nodes, was optimized to provide the best numerical results. An unstructured mesh could also be used for more complex geometry, but the use of different meshes could raise problems of interpolation between the two grids since calculations are performed at different mesh points. FEM computations are made at integration points and FVM at the centre of the mesh. Flux-expert® must provide the Joule effect losses and current densities at the centres of the Fluent® mesh volumes; Fluent® therefore first sends the centre coordinates of its mesh volumes, and Flux-expert® locates them on its mesh. At each subsequent iteration it can thus interpolate the physical data before sending them to Fluent®. The point location method in finite element meshing consists in determining the element number E containing the point and the reduced coordinates of point $\vec{u}$ to be located in element E.

The reduced coordinates of the real element point at the previous coordinates is given by the T application (12) defined by the reference element in the real element. The T application is built from Lagrange polynomials and is defined by the correspondence of nodes between the real and reference elements:

$$T : \vec{u} \in \mathrm{Re}f \rightarrow \vec{x} \in \mathrm{Real}/\vec{x}(\vec{u}) = \sum_{k=1}^{NBN} \alpha_k(\vec{u})\vec{x}^k \qquad (12)$$

Locating the $\vec{X}$ point requires determining the $\vec{u}$ solution of the generally non-linear system (13) solved by the Newton–Raphson method [26].

$$\sum_{k=1}^{NBN} \alpha_k(\vec{u})x_i^k = X_i \qquad (13)$$

This method is used to locate the centres of control volumes where Flux-Expert® has to calculate the volume density Joule losses appearing in the term of Eq. 6. For the current density calculation and the surface Joules losses Q_S, the preceding method must be adapted to locate on a finite element set the volume centres of the zone in which hydrogen is released.

Surface elements have 2D elements reference. The $\vec{u}$ vector should only have two constituents: the space variables tangent to the element. To correct this difficulty, a thickness unit was applied to the surface elements during the location by building nodes in the transverse face direction (Fig. 5), resulting in a plane-parallel volume element of which the primordial surface element constitutes a section. For the nodes of this new element, a family

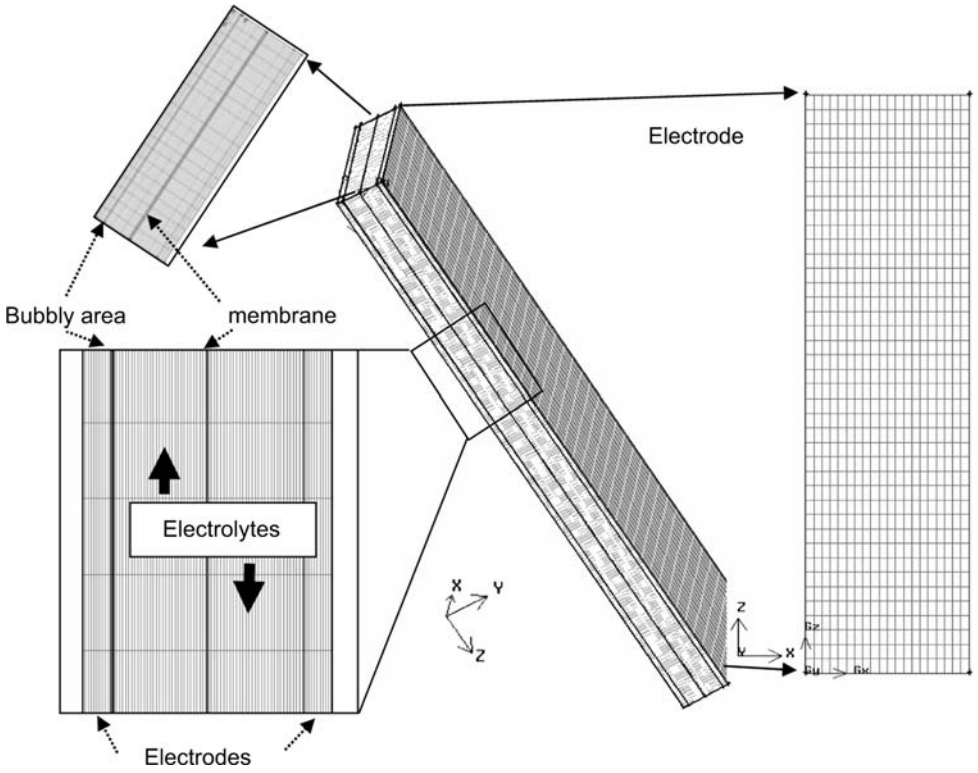

Fig. 4 Grid used for thermo hydraulic and electro kinetic modelling

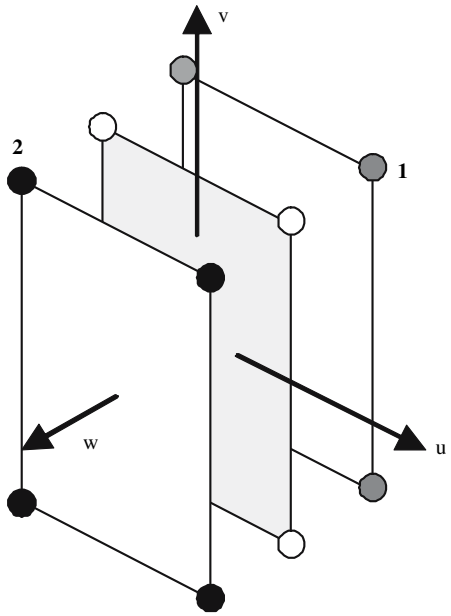

Fig. 5 Surface element thickness for point location

of Lagrange polynomial β is defined in reduced coordinates u, v, *and* w as follows:

$$\beta(u, v, w) = \alpha(u, v)\gamma(w) \tag{14}$$

$\alpha(u, v)$ are the Lagrange polynomials associated with the surface element nodes and $\gamma(w)$ are additional Lagrange polynomials used to give an element thickness. For nodes situated at $w = -1$, γ is defined as:

$$\gamma_1(w) = 0.5(1 - w) \tag{15}$$

and for nodes situated at $w = +1$

$$\gamma_2(w) = 0.5(1 + w) \tag{16}$$

The remainder of the location algorithm is similar to the preceding explanation. Only the u and v components of the reduced coordinates are retained; the third component w concerns the distance in the element.

In this work the mesh size was the subject of particular attention. Caire et al. [21] showed that the secondary distribution of potential is particularly sensitive to the grid length. This effect is due to the post-processing from the unknown factor potential V of current density J which mainly contributes to coupling in terms of mass and heat transfers (see Eq. 18). In the same way, the Fluent® grid must be particularly well done to properly describe the bubble evolution and biphasic drainage.

4.4 Electrochemical computational choices

The interfacial electrode/electrolyte potential discontinuity η is related to the local normal current density by Tafel's law [17], obtained from [10]:

$$\eta = -0.275 + 0.892 \log_{10} \left\| \vec{J} \bullet \vec{n} \right\| \quad (17)$$

In every point of the study set the current density $\vec{J}$ is related to the potential V as follows:

$$\vec{J} = -\sigma \vec{\nabla} V \quad (18)$$

The same iterative algorithm described precisely in [8] was used to compute the local current density on the cathode.

4.5 Thermo hydraulic computational choices

An Euler–Euler model is generally used to describe two-phase flow in presence of scattered bubble drainage [5, 24]. For all the trials in different geometry conditions and electrolyte velocities encountered, the gas and liquid Reynolds numbers were always greater than 1300 and a turbulent model was systematically used. To describe the sulphuric acid/hydrogen gas biphasic mixture the so called realizable $k-\varepsilon$ Euler-Euler model of Fluent® [27] was chosen because it gives realistic turbulent drainage even in the case of major pressure variations as in this filter press electrolyser.

5 Modelling results

All the results presented here concern the quadrangular 0.04 × 0.013 × 0.16 m filter press electrolyser shown in Fig. 1. They were obtained after the usual checks for two-phase flow computations: the grid meshes were carefully refined to give grid-independent results and the inlet-outlet mass balances for electrolyte and hydrogen were verified.

5.1 Code coupling behaviour

The interaction between the two codes is demonstrated by the convergence of the computational residuals with successive iterations. The residual available in Fluent® is defined as (19):

$$\text{Residual} = \sqrt{\left| \frac{A_{i+1} - A_i}{A_i} \right|} \quad (19)$$

where A_i is the value of variable A at iteration i.

As two-phase flow models are more complex to solve than electro kinetic models, exchanges between the two codes are performed at each iteration for Flux Expert® and only every 20 iterations for Fluent®.

Figure 6 shows the variation of the residuals in Fluent® from iteration 1 to iteration 180 (due to the chosen 20:1 ratio, data transfers from Flux Expert® to Fluent® correspond to iterations 1–9 in Flux Expert®). The choice of this ratio was not trivial since the computation time is much longer in Fluent® and the exchange of data is time-consuming: the proper ratio appeared after some trials as a good trade off to ensure the rapid convergence of data exchanged between the two codes. The curve shape illustrates the quality of the system convergence. During the first exchange after 20 iterations of Fluent®, the codes exchange the coordinates of the integration points, after which the physical values are exchanged. A sudden increase in the residuals is observed after 40 iterations in Fluent®, i.e. at the second iteration for Flux Expert®, corresponding to the transmission of fresh data between the two codes. A similar observation can be made for the temperature evolution in Fig. 7: for example, a temperature step of decreasing amplitude with each data exchange between the two codes confirms the convergence of the temperature parameter.

This convergence behaviour is quite satisfactory for so complex a model, although 180 iterations were required to obtain satisfactory precision on the temperature. The computation lasted 24 h using a Pentium IV PC for Flux Expert® and a Core 2 Duo PC for Fluent®, both running Linux, and connected to the CEA corporate network.

5.2 Results of heat transfer and fluid mechanics computations

The initial results concerning the thermo hydraulic behaviour of the filter press electrolyser are shown under

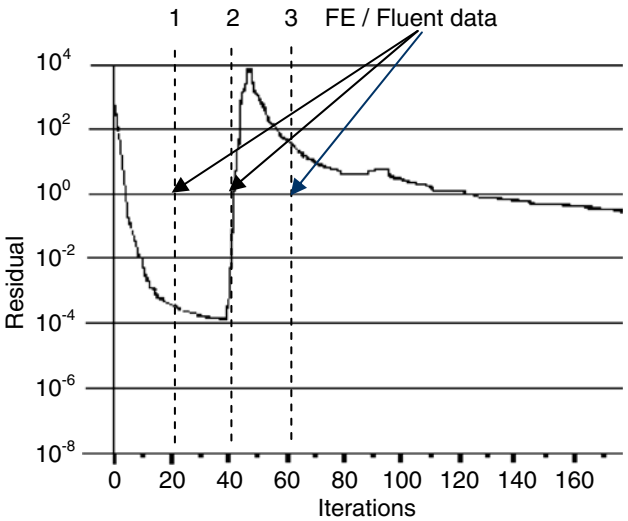

Fig. 6 Evolution of residual over 180 iterations in Fluent®

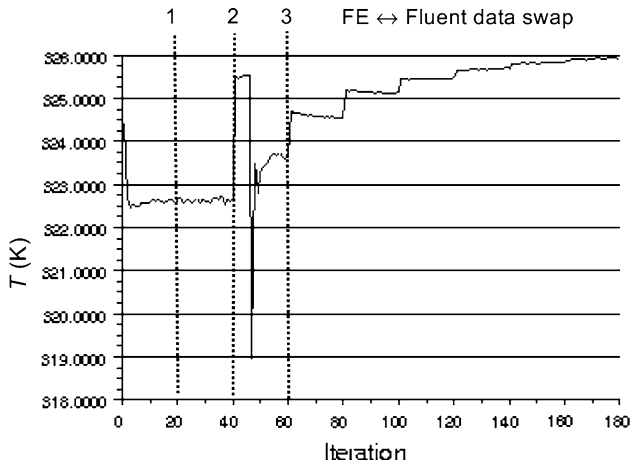

Fig. 7 Mean temperature evolution at each Fluent® iteration

operating and modelling conditions that are subject to further optimization and improvement in subsequent work. The thermal behaviour of the electrolyser is shown in gray scale in Fig. 8.

The temperature depends on the volume heat sources due to Joule effect losses, convective transport in the counter current liquid flows, and heat exchange by conduction in the solids and liquids. A cross-sectional view of the electrolyser through the middle of each compartment provides a better indication of the temperature rise versus height.

Figure 9 shows a temperature evolution in both electrolyser compartments comparable to that observed in the

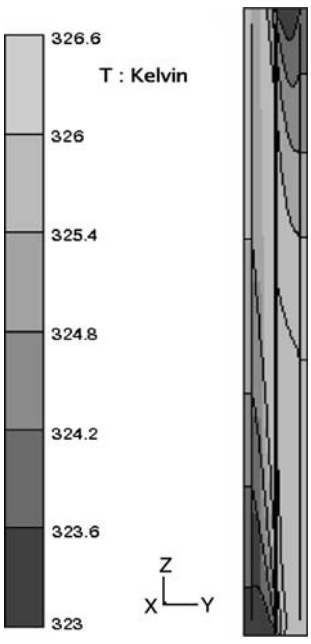

Fig. 8 Gray scale temperature map

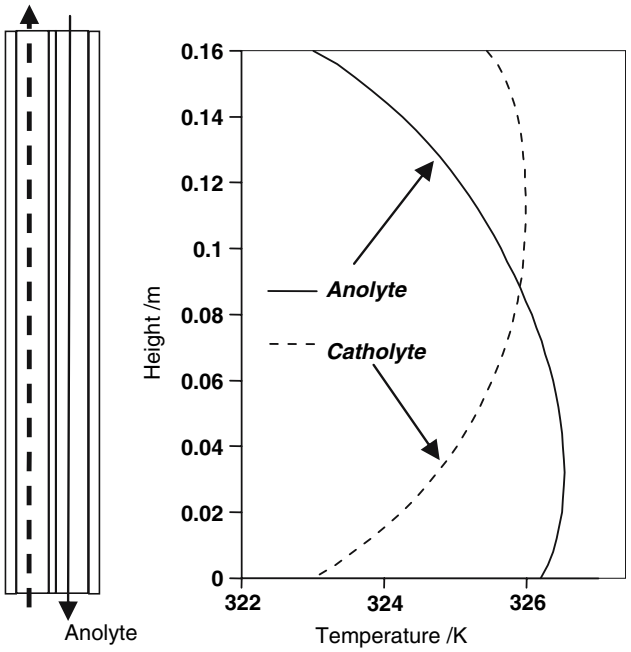

Fig. 9 Temperature versus height in the anolyte and catholyte

cold and hot compartments of a plate-type heat exchanger with a counter current fluid evolution [28]. Here, the temperature increases by 4 K between the coldest point (liquid inlets) and the hottest (anolyte outlet). The temperature rise inside the electrolyser reaches a maximum where the electrical conductivity of the cell is the lowest (area of larger gas fraction), and where the liquid flow velocity is also the lowest (catholyte).

For lack of precise experimental data, the results shown here do not yet take into account the surface heat sources generated by over potentials, although their effect on the temperature can be estimated at about 6–8 K given the over potentials obtained (see paragraph 4.4). Similarly, it would be of interest in future calculations to take into account the heat produced by exothermic reactions such as dissolution in the anolyte of the H_2SO_4 formed by oxidation of SO_2. The temperature will be recomputed with greater accuracy when the experimental results are obtained. Nevertheless, the estimated temperature evolution is already compatible with the materials used and should maintain corrosion within acceptable limits. This is an important result for the feasibility of the electrolyser.

5.3 Results of two-phase flow calculations with Fluent®

Fluent® allows the use of a partial mass source that represents the electrochemically produced hydrogen. The gas is known to be released in this electrolyte at the cathode in

bubbles 100 μm in diameter [2], is transported by the bath and exits at the top of the electrolyser.

Figure 10 illustrates the hydrogen evolution along the interface between cathode and the sulphuric acid solution (catholyte); due to the combined fluid transport and bubble release at cathode, the gas volume fraction increases along the cathode wall. It is interesting to note that the bubble plume proposed by the first model appears localized at the cathode/catholyte interface. Similar results were observed experimentally by Wetind [15] and modeled by Dahlkild [29]. The local gas volume fraction reaches its maximum (13%) at 0.6 mm from the cathode surface. As expected the hydrogen volume fraction is much lower than the 74% maximum value of rigid spherical hydrogen bubbles assumed to be stacked in a hexagonal close-packed or face-cantered cubic structure [17]. Nevertheless a 50% volume fraction can be reached with specific flow drainage [18]. Note that the maximum hydrogen concentration tends to move away from the cathode face. This result is characteristic of a bubble plume. All these numerical results are similar to Wetind's experimental observations in the case of hydrogen released in a chlorate electrolyser [15].

The velocity vector plot in Fig. 11 shows the influence of the gas volume fraction on the electrolyte flow velocity in the catholyte compartment compared with the anolyte compartment in which there is no gas release.

The velocity in the anode compartment varies only slightly and tends toward two parabolic profiles since there is no bubble evolution at the anode. This hydraulic velocity shape is characteristic of the wall effect. The velocity in the cathode compartment varies significantly with the gas volume fraction: the greater the quantity of evolving gas bubbles, the higher the velocity along the electrode. At a constant feed rate, this observation is directly related to the apparent restriction of the free flow cross section. The maximum velocity reached is 0.16 m s^{-1} compared with an inlet value of 0.1 m s^{-1}; this represents a slight increase in the electrolyte velocity in the cathodic compartment favourable to the overall heat and mass transfers in the filter press reactor.

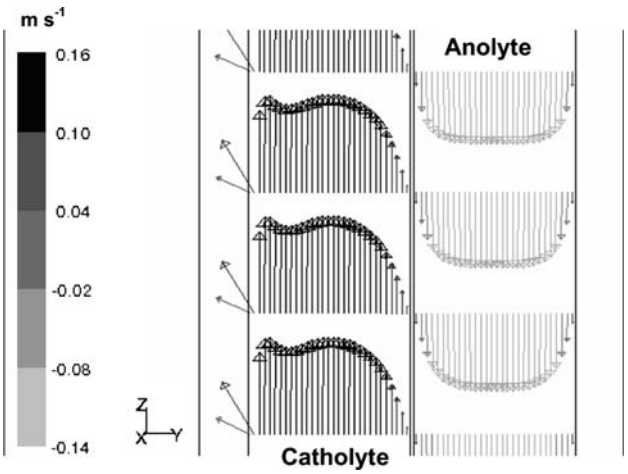

Fig. 11 Vector plot of electrolyte velocity (m s^{-1}) at the top of the cell

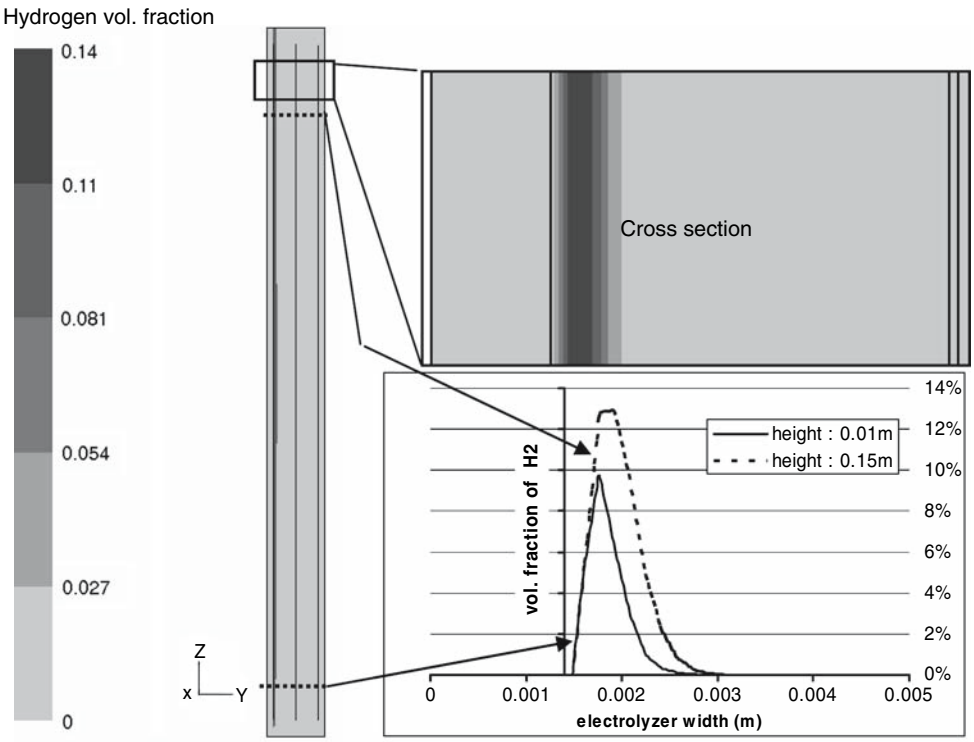

Fig. 10 Gray scale and horizontal cross section representations of gas volume fraction

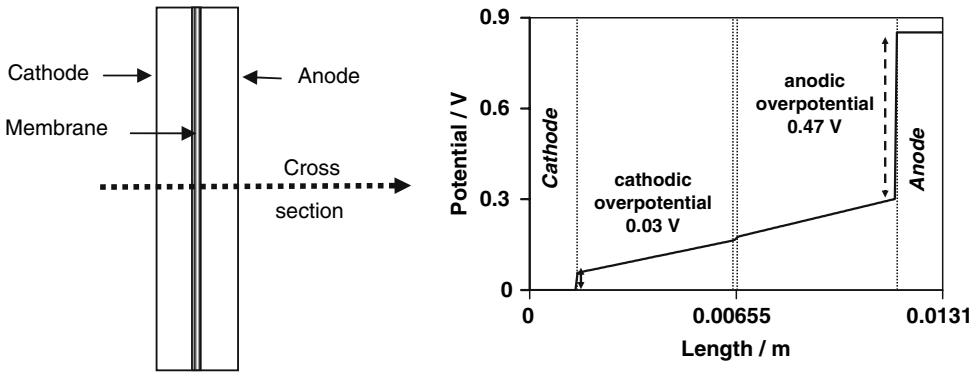

Fig. 12 Electrical potential variation in the cell

5.4 Results of electro kinetic simulations

The data supplied to Flux Expert® by Fluent® are used to calculate the electrical potential of the cell taking into account the gas volume fraction and the local temperature. The potential convergence appeared to be faster than temperature and velocity convergence. The secondary current distribution reveals a relatively large anodic over potential due to the irreversibility of electrochemical oxidation of SO_2 to H_2SO_4. This phenomenon is detailed in the cross section by plotting in Fig. 12 the potential variation at the centre of the electrolyser along a horizontal path.

The dotted path between cathode and anode shows the individual contributions to the overall potential of the electrolysis cell. Here the anode over potential accounts for 70% of the cell potential, although hydrogen production results in a potential drop of 30 mV, or only 4% of the cell potential. This result shows that the overall cell voltage is essentially limited by the anode over potential as in fluorine or aluminium electrolysers [8, 18–20]. Although this initial numerical result must be improved by incorporating more precise experimental Tafel laws, it highlights the importance of optimizing the anode over potential to lower the overall cell voltage and thus the cost of hydrogen mass production by the Westinghouse process.

6 Conclusions

The model described here was designed to simulate the operation of an electrolyser which is a fundamental component in the Westinghouse process for producing hydrogen by a hybrid electrochemical-thermo chemical cycle at the high temperatures given by the forthcoming VHT reactor. The filter press electrolyser selected for its compact size was modelled by coupling the Fluent® and Flux Expert® codes. This approach allowed us to take into account under optimum conditions both the electrochemical phenomena (over potentials in particular) and the complex two-phase flow due to hydrogen production at the cathode. The calculations showed the significant influence of fluid mechanics and gas production on the reactor heat transfer properties. The fluid flow velocity along the cathode increased slightly in the reactor, by a factor of 1.6, due to the release of hydrogen bubbles. This finding is of particular importance for the preliminary design of a future fully optimized electrolyser and was one of the principal results obtained by coupling the Flux-Expert® and Fluent® codes.

The overpotentials and highly exothermic chemical reactions were not taken into account with sufficient accuracy for lack of precise experimental data, but the coupled model is capable of doing so without difficulty when they are soon measured. The initial calculations showed that the plume of hydrogen bubbles might be slightly too narrow. This is due to the lack of a suitable description of the bubble–bubble interactions that determine the shape of the plume in electrolysers [25]. Population balance models allowing for bubble coalescence and break up should also be taken into account through the development of specific physical operators [19–20]. Finally, the two-phase flow model will be calibrated and refined from gas fraction measurements along the cathode in the future laboratory pilot device specified and designed from this model.

References

1. Gauthier JC, Brinkmann G, Copsey B, Lecomte M (2006) Nucl Eng Des 236:526–533
2. Vitart X, Le Duigou A, Carles P (2006) Energy Conversion Manag 47:2740–2747
3. Brecher LE, Wu CK (1975) US Patent No 3,888,750 assigned to Westinghouse Electric Corporation
4. Brecher LE, Spewock S, Warde CJ (1977) Int J Hydrogen Energy 2:7–15
5. Agranat S, Zhubrin AM, Hinatsu J, Stemp M, Kawaji M (2006) European fluids engineering summer meeting July, Proceedings of FEDSM 2006 ASME Joint U.S., Miami, FL, pp 17–20
6. Jomard F, Feraud JP, Morandini J, Du Terrail Couvat Y, Caire JP (2007) Modeling a filter press electrolyzer for the Westinghouse

hybrid cycle using two coupled codes, International Conference on Nuclear Engineering, Nagoya, Japan, Proceeding ICONE15-10639
7. Goosen JE, Lahoda EJ, Matzie R, Mazzoccoli JP (2003) Improvements in Westinghouse process for hydrogen production, pp. 1509–1513
8. Roustan H, Caire JP, Nicolas F, Pham P (1998) J Appl Electrochem 28:237–243
9. Struck BD, Junginger R, Boltersdorf D, Gehrmann J (1980) Int J Hydrogen Energy 5:487–497
10. Lu PWT, Ammon RL (1980) J Electrochem Soc 127(12):2610–2616
11. Coeuret F, Storck A (1993) Eléments de génie électrochimique, Technique & Documentation, Lavoisier, Paris
12. Hwang JJ, Wu SD, Lai LK, Chen CK, Lai DY (2006) J Power Sources 161:240–249
13. Jomard F, *DRT* (2002) Prédimensionnement par modélisation numérique de l'électrolyseur de production d'hydrogène du cycle hybride Westinghouse, INPG, Grenoble
14. Atey BG, El Shakre ME (1983) J Appl Electrochem 14(3):367–371
15. Wetind R (2001) Ph.D. Thesis, Royal Institute of technology, Two-phase flows in gas-evolving electrochemical applications Stockholm
16. Shih TH, Liou WW, Shabbir A, Yang Z, Zhu J (1995) A new k–ε eddy-viscosity model for high Reynolds number turbulent flows, model development and validation. Comput Fluids 24(3): 227–238
17. Arnaud P (1988) Cours de chimie physique. Dunod, Paris
18. Vogt H (1999) J Appl Electrochem 29(10):1155–1159
19. Vogt H (1997) Electrochimica Acta 42(17):2695–2705
20. Vogt H (1999) J Appl Electrochem 29(10):137–145
21. Caire JP, Chifflet H (2002) Environmetrics 13(1):1–8
22. Eigeldinger J, Vogt H (2000) Electrochimica Acta 45(27):4449–4456
23. Clift R, Grace JR, Weber ME (1978) Bubbles, drops and particles. Academic Press, NY
24. Espinasse G, Peyrard M, Nicolas F, Caire JP (2007) J Appl Electrochem 37:77–85
25. Mandin P, Wüthrich R, Hamburger J, Picard G, Diphasic (2005) Electrolysis process modelling for a vertical electrode. Proceedings of the 7th European symposium on electrochemical engineering, Toulouse, France
26. Nougier JP (1991) Méthodes de calcul numérique, 3e edn. MASSON, Paris
27. Fluent (2005) Users manual, chapter 24
28. Caire JP, Roure A (2007) Pre design of a molten salt thorium reactor loop. 15th International conference on nuclear engineering, Nagoya, Japan, Proceeding ICONE15-10493, April 22–26, 2007
29. Dahlkild AA (2001) J Fluid Mech 428:249–272